Monatsh Chem 139, 999–1003 (2008)
DOI 10.1007/s00706-008-0893-5
Printed in The Netherlands

Monatshefte für Chemie
Chemical Monthly

Oxygen bubble mould effect: serrated nanopore formation and porous alumina growth

Xufei Zhu, Lin Liu, Ye Song, Hongbing Jia, Huadong Yu, Xuemei Xiao, Xiuli Yang

School of Chemical Engineering, Nanjing University of Science and Technology, Nanjing, China

Received 11 December 2007; Accepted 11 January 2008; Published online 18 February 2008

Abstract We discovered a unique formation of serrated nanopore in porous anodic alumina (PAA). A new growth model is proposed for the formation mechanism of PAA. The model emphasizes the close relationship between pore generation and oxygen evolution. The initial pore formation is ascribed to oxygen bubble mould effect. Our model provides a satisfactory explanation for the growth process of PAA, alleviating the difficulties encountered in existing theories. These findings represent a decisive new step towards the full understanding of the nature of PAA films. The serrated nanopore arrays in PAA could also be used in a wide range of future nanostructure fabrications.

Keywords Anodic alumina; Formation mechanism; Nanostructures; Oxygen evolution.

Introduction

Porous anodic alumina with ordered nanopores has received considerable attention because it can be used as a template or host material for the development of nanostructures [1–3]. In the past decade, various functional nanomaterials had been developed utilizing such a template, which were involved in magnetic recording media [4], nanoelectrodes [5], photocatalysis [6], biosensors [7], thermoelectric materials [8], separation membranes [9], *etc*. Porous anodic alumina had been studied extensively over five decades [10–15]. But, the formation mechanism of the highly ordered pore structures is not yet clear to date [16, 17].

Previous studies of anodic aluminum oxide have shown that two types of anodic films on aluminum exist, the nonporous barrier anodic alumina (BAA) and the porous anodic alumina (PAA) [14, 17]. Anodized in neutral solutions, aluminum can form flat, featureless insulating BAA. Whereas anodized in acid solutions (*e.g.*, phosphoric and oxalic acid), it can form PAA with an ordered array of pores [12, 17]. Many researchers [10–13] have been investigating PAA growth mechanism, while others [15–18] have successfully fabricated PAA with perfect nanopore arrays for nanostructure template application. Several possible mechanisms have been proposed to explain its ordered hexagonal porous structure. So far, the widely approved viewpoint is that initial pore nucleation undergoes a field-assisted chemical dissolution on BAA layer surface, and pore development is due to redistribution of current and a field-assisted hydrogen ion attack on the pore bottom [12–14, 17]. However, the nature of PAA growth is far from being fully understood [14, 16, 17]. Recently, in the study of aluminum anodization in H_3PO_4 solutions, we discovered PAA film with regular serrated nanopores (Fig. 1). Unfortunately, the existing theories of PAA cannot be applied to explain the formation of such serrated nanopores. In this paper,

Correspondence: Ye Song, School of Chemical Engineering, Nanjing University of Science and Technology, Nanjing 210094, China. E-mail: soong_ye@sohu.com

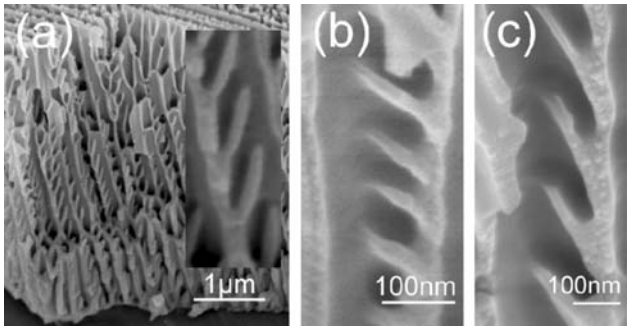

Fig. 1 SEM micrographs showing the cross-section view of the serrated nanopores in alumina film. (a) Anodized for 3000 s in 10 wt% H_3PO_4 aqueous solution. Inset, magnified image for one of the serrated nanopores. (b) Anodized for 3000 s in 6 wt% H_3PO_4 aqueous solution. (c) Anodized for 3000 s in 6 wt% H_3PO_4 in solvent mixture of 50 wt% ethylene glycol (*EG*) and 50 wt% H_2O

we report this novel morphology of PAA film and propose a new model for the formation mechanism of PAA film.

Results and discussion

Figure 1 gives the SEM images of PAA anodized in H_3PO_4 solutions for a long time (3000 s). Serrated nanopores can be clearly found within the PAA film. To the best of our knowledge, this is the first demonstration for this unique PAA film.

We believe that the formation of the serrated nanopores is related to oxygen gas generation during aluminum anodization. In fact, it is well known that the growth of anodic films on aluminum is generally accompanied by the generation of oxygen bubbles. Some authors [19] have demonstrated that oxygen gas can be generated within BAA films on some dilute binary aluminum alloys. We previously reported that the PAA film was also able to grow in BAA film-forming electrolyte because of the evolution of oxygen gas [20]. Other authors [21] also found cellular PAA grown in neutral organic electrolyte. These findings implied that the field-assisted chemical dissolution is not the only mechanism for the PAA formation. Oxygen gas generation is likely to play a crucial role in this respect as well. Unfortunately, the phenomenon of oxygen gas evolution during anodizing had been ignored by most researchers for a long time. It is worth noting that porous metal deposits in cathode can be created by a hydrogen co-evolution process [22]. Here, we will focus on studying the growth of PAA in H_3PO_4 solutions in ethylene glycol (*EG*) and pay close attention to the effect of oxygen generation on aluminum anodization.

Figure 2 shows the SEM images of PAA formed in H_3PO_4 solutions. It is noted in Fig. 2a–d that many pores are closed to the film surface. Their presence can not be explained fully by field-assisted dissolution mechanism. We ascribe these pores to the evolution of oxygen, and simply call them oxygen bubble-induced pores (OBIPs). It should be noted that most of the previous anodization experiments were conducted on electropolished aluminum [13–18, 21]. Thus, it is not easy to distinguish which pores are OBIPs among others due to the field-assisted dissolution (FAD) simultaneous occurring

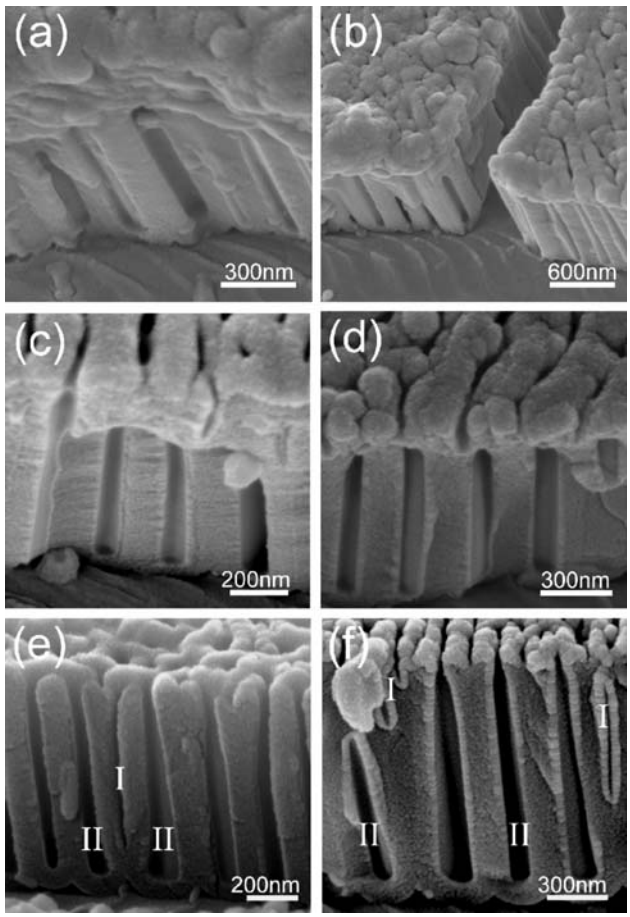

Fig. 2 Two types of pores in PAA films: induced by electric field-assisted dissolution and by oxygen bubbles. (a) Anodized for 300 s in 6 wt% H_3PO_4 in *EG* solution. (b) The same sample as (a) in different observation region. (c) Anodized for 300 s in 2 wt% H_3PO_4 in *EG* solution. (d) Anodized for 500 s in 4 wt% H_3PO_4 in *EG* solution. (e) Anodized for 165 s on electropolished aluminum in 6 wt% H_3PO_4 in *EG* solution. (f) Anodized for 300 s in 6 wt% H_3PO_4 in solvent mixture of 75 wt% *EG* and 25 wt% H_2O

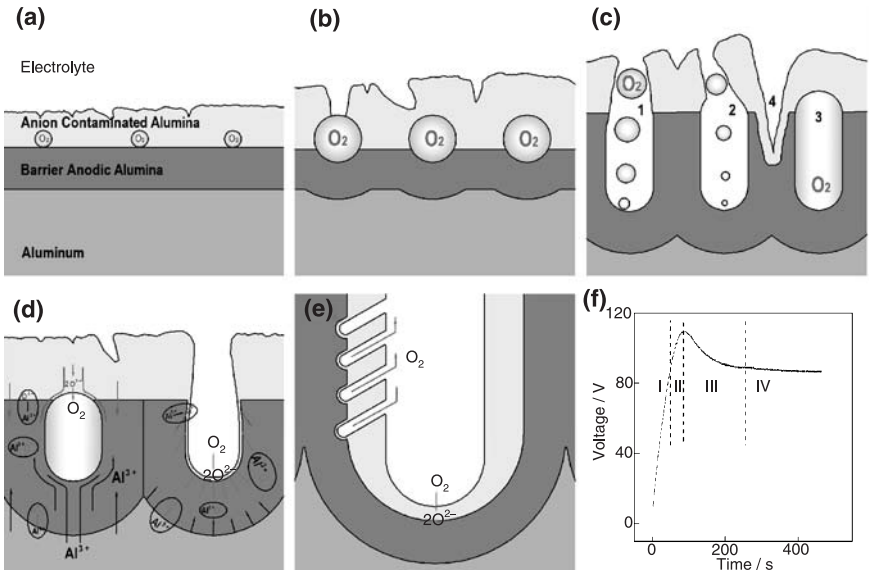

Fig. 3 New PAA model showing the early stage of pore formation and the serrated nanopores formation. (a) Three interfaces appear in the oxide film. (b) The oxygen bubble mould effect (OBME) gives rise to the formation of hemispherical shape for a pore bottom. (c) Further evolution of pores in (b). Most of the oxygen bubbles are connected with the outer electrolytes through the dissolution pit bottom. The No. 1 and 2 pores with regularity are OBIPs perforated by FAD. The No. 3 closed pore is an OBIP. The No. 4 pore with irregular configuration is caused solely by FAD. (d) Schematic diagram of the migration path of anions and cations as well as oxide growth in the two cases: electrolytes have not penetrated into pores yet, then the OBME gives rise to the oxide growth embracing the bubble mould (*left*) and electrolytes have penetrated into pores (*right*). (e) Schematic diagram of the formation of serrated nanopores. (f) Typical voltage-time response for aluminum anodized at $7\,\mathrm{mA}\cdot\mathrm{cm}^{-2}$ in H_3PO_4 solutions

on aluminum surface. Therefore, in this study, we purposely stayed with the natural oxide film on aluminum in order to retard FAD process, giving us an opportunity to study OBIPs carefully.

Because of the absence of a natural oxide layer, all pores shown in Fig. 2e are open to the surface, as one would anticipate. The pore marked ''I'' is without a round bottom and broadens towards the film surface. It is obviously dissimilar to the other smoothly columnar pores (marked ''II''), which we regarded as OBIPs whereas pore ''I'' was induced by FAD. With the presence of natural oxide film, these two types of pores were also observed. Such is the case shown in Fig. 2f for the film formed in aqueous electrolytes on aluminum with a natural oxide film.

Based on the above experiment findings, we put forward a new growth model of PAA, schematically depicted in Fig. 3.

In the initial period of galvanostatic anodizing, a BAA film is formed rapidly though acidic dissolution of oxide also exists simultaneously. As the BAA film thickens, the outermost layer of the oxide film will be contaminated by electrolyte species where the passage of ions is believed to proceed relatively easily [12]. Then, three interfaces appear in the oxide film (Fig. 3a), *i.e.*, electrolytes/anion-contaminated alumina (ACA) interface, ACA/BAA interface, BAA/aluminum interface. In this initial stage, the forming voltage rises linearly with time, which implies that the efficiency of film growth is close to 100%. The current through the BAA layer is mainly ionic, whereas the electronic current can be neglected. In other words, the anodic current is principally used to form oxide, and oxygen evolution, if any, is very limited (Fig. 3f, stage I). However, while the film grows to a certain thickness or the forming voltage reaches a certain value, avalanche electronic currents through BAA layer by an impact ionization mechanism will dominate. The avalanche electron multiplication process due to high electric field leads to an exponential growth of the electronic current, obeying the following equation [23]:

$$j_e = j_0 \exp(\alpha d) \tag{1}$$

where α (cm^{-1}) is the impact ionization coefficient, d (cm) the oxide thickness, and j_0 ($\mathrm{mA}\cdot\mathrm{cm}^{-2}$) the primary electronic current of the avalanche related to the electrolyte species incorporated into the oxide

[24]. Thus, the electronic current gives rise to the evolution of oxygen gas by the oxidization of O^{2-}/OH^- enriched in the ACA/BAA interface (Fig. 3a). Under the condition of constant current anodization, the enhancement of the electronic current consequentially leads to the decrease of the ionic current, resulting in the decline of film growth rate and the increase of oxygen evolution rate. With further anodizing, oxygen bubbles begin to accumulate at some sites of the ACA/BAA interface due to the shielding by the upper ACA layer (Fig. 3a). At the same time, the anodic oxide will continue to develop at the bubble-free sites near the ACA/BAA interface but be arrested at the bubble-occupying sites. The oxygen bubbles are approximately spherical and grow in size as the anodic film thickens.

As a result, the oxygen bubbles can behave as a mould during the film growth (Fig. 3b). Two mould effects are presented. One is to exert pressure on the BAA layer, causing a hemispherical indentation on the BAA layer because of the plasticity of anodic alumina [24] and high pressure of the bubbles [20], which is the precursor of regular-shaped pores in PAA films. The other is to change the migration path of anions and cations. The Al^{3+} egress and O^{2-}/OH^- ingress must migrate around the bubbles, which leads to the growth of oxide as shown in Fig. 3d. In the meantime, the local dissolution of oxide is also proceeding with film growth. Some dissolution pits will appear at first in the ACA layer to connect some oxygen bubbles with the outer electrolytes through the pit. But the bubbles are not released immediately due to the pressure of the solutions (Fig. 3b). Consequently, the voltage continues to increase with time but the slope is progressively reduced (Fig. 3f, stage II). The bubbles still have the mould effect until the pressure of the bubbles is higher than that of the solutions. Once the bubbles are released, the electrolytes will penetrate into the initial pores formed by the oxygen bubbles (Fig. 3c). This is effectively equivalent to a decrease of the mean BAA thickness, and thus the voltage begins to drop from its maximum value. When all bubbles have been liberated due to perforation by local oxide dissolution or they simply burst out of the ACA layer (Fig. 4), a steady voltage is reached. This corresponds to a decrease of voltage from the peak to a plateau on the voltage-time curve (Fig. 3f, stage III). This voltage-time response plateau implies a dynamic equilibrium between anodic oxide growth and field-assisted dissolution [14]. A steady-state pore structure is eventually formed by closely packed cylindrical cells, each containing a central pore separated from the aluminum metal by a layer of scalloped hemispherical barrier oxide (Fig. 3f, stage IV).

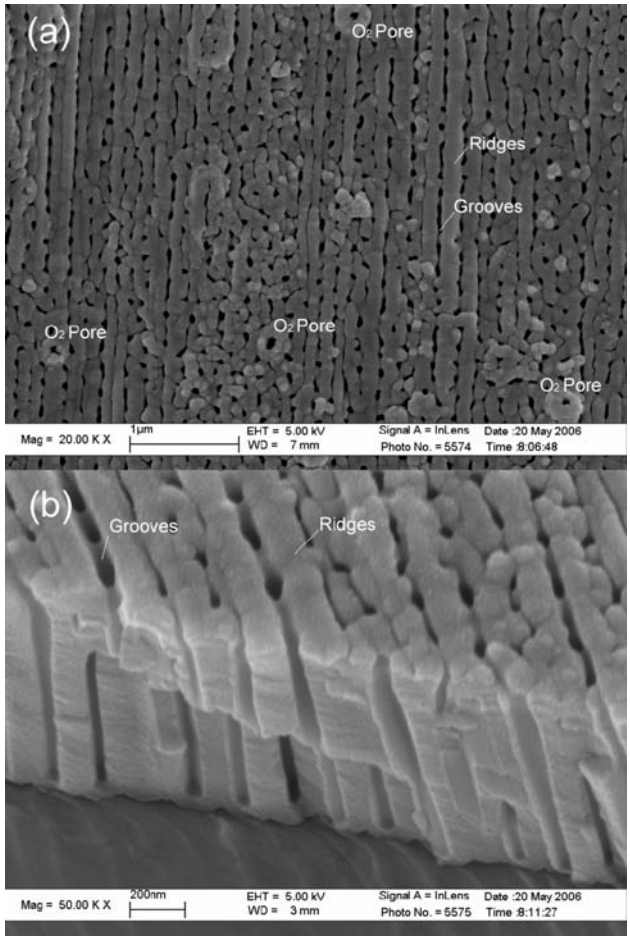

Fig. 4 Trace left by oxygen bubbles bursting out of the ridges on film surface. Aluminum was anodized in 6 wt% H_3PO_4 *EG* solution for 500 s. (a) Surface SEM micrograph of the prepared film. (b) Cross-sectional SEM micrograph of the same sample

In the meantime, the ACA/BAA interface still exists after the steady-state pore structure is formed. With the considerations mentioned above, the oxygen gas should continue to be generated at this interface in the pore wall of the PAA film, thus resulting in pore formation in the pore wall due to the OBME as well (Fig. 3e). This is the main process for the formation of the serrated nanopores described above in Fig. 1.

In conclusion, we believe that PAA films with regular pores are mainly produced by the OBME, primarily because the factors affecting the pore

structure are exactly the same as those influencing oxygen evolution. The present results may provide a decisive step towards a thorough understanding of PAA film. We also anticipate that the OBME may shine some light upon the yet-unclear formation mechanisms of other porous materials such as anodic silica [25] and titanium oxide [26], which are extensively used in optoelectronics and bioelectronics [27]. Furthermore, the newly discovered PAA film with ordered serrated nanopores, as reported here, may be used as a novel template for advanced nanomaterial development.

Experimental

Aluminum samples, $20 \times 7\,mm^2$, were cut from 200 μm thick, fully annealed high-purity (99.99%) aluminum sheets. The samples were degreased by ultrasonication in acetone for 10 min and then a thorough rinse in deionized water. In order to eliminate the influence of natural oxide film on aluminum surface, some samples were electropolished under a constant current density condition of $50\,mA \cdot cm^{-2}$ at 23°C for 200 s in a mixture of perchloric acid and ethanol (1:4 *v*/*v*). Unless otherwise stated, samples with a natural oxide film were used in this study without electropolishing treatment.

Anodization at a constant current density at $7\,mA \cdot cm^{-2}$ was carried out in corresponding electrolytes at room temperature under normal atmosphere pressure, using an aluminum counter electrode. Solutions were prepared from reagent grade chemicals and deionized water. Unless specially noted, the electrolyte temperature was purposely not controlled during anodizing, but the maximum temperature never exceeded 60°C. The voltage-time responses during anodizing were recorded automatically by a computer measurement system described elsewhere [28].

The anodized samples were examined by scanning electron microscopy (SEM, LEO-1530VP). The cross-sectional SEM images of alumina film were obtained by the following procedure. The anodized specimen was bent into a V-shape, producing cracks in the oxide film. The SEM observation was conducted from the crack section of alumina film. It is worth mentioning that this specimen-preparation technique avoids the potential damage to alumina film morphology due to ultramicrotomy for TEM. In addition, since PAA formed in aqueous solutions was not as easy to be cracked as that formed in ethylene glycol (*EG*) solutions, the electrolytes employed in this study were mainly *EG* solutions.

Acknowledgements

We thank *Robert Y. Ting* (University of Central Florida) for a very close reading of this manuscript and extensive revisions. This research was supported by the National Natural Science Foundation of China (No. 50572039).

References

1. Masuda H, Fukuda K (1995) Science 268:1466
2. Hobbs KL, Larson PR, Lian GD, Keay JC, Johnson MB (2004) Nano Lett 4:167
3. Tian M, Xu S, Wang J, Kumar N, Wertz E, Li Q, Campbell PM, Chan MHW, Mallouk TE (2005) Nano Lett 5:697
4. Whitney TM, Searson PC, Jiang JS, Chien CL (1993) Science 261:1316
5. Taberna PL, Mitra S, Poizot P, Simon P, Tarascon J-M (2006) Nature Mater 5:567
6. Chu SZ, Wada K, Inoue S, Todoroki S (2002) Chem Mater 14:266
7. Matsumoto F, Nishio K, Masuda H (2004) Adv Mater 16:2105
8. Sander MS, Prieto AL, Gronsky R, Sands T, Stacy AM (2002) Adv Mater 14:665
9. Yamaguchi A, Uejo F, Yoda T, Uchida T, Tanamura Y, Yamashita T, Teramae N (2004) Nature Mater 3:337
10. Keller F, Hunter MS, Robinson DL (1953) J Electrochem Soc 100:411
11. Spooner RC, Forsyth WJ (1963) Nature 200:1002
12. Thompson GE, Wood GC (1981) Nature 290:230
13. Furneaux RC, Rigby WR, Davidson AP (1989) Nature 337:147
14. Thompson GE (1997) Thin Solid Films 297:192
15. Lee W, Ji R, Gösele U, Nielsch K (2006) Nature Mater 5:741
16. Masuda H, Hasegwa F, Ono S (1997) J Electrochem Soc 144:L127
17. Li FY, Zhang L, Metzger RM (1998) Chem Mater 10:2470
18. Asoh H, Ono S, Hirose T, Nakao M, Masuda H (2003) Electrochim Acta 48:3171
19. Zhuravlyova E, Iglesias-Rubianes L, Pakes A, Skeldon P, Thompson GE, Zhou X, Quance T, Graham MJ, Habazaki H, Shimizu K (2002) Corros Sci 44:2153
20. Zhu XF, Li DD, Song Y, Xiao YH (2005) Mater Lett 59:3160
21. Liu Y, Alwitt RS, Shimizu K (2000) J Electrochem Soc 147:1382
22. Shin H-C, Dong J, Liu M (2003) Adv Mater 15:1610
23. Albella JM, Montero I, Martinez-Duart JM (1987) Electrochim Acta 32:255
24. Skeldon P, Thompson GE, Garcia-Vergara SJ, Iglesias-Rubianes L, Blanco-Pinzon CE (2006) Electrochem Solid-State Lett 9:B47
25. Frey S, Grésillon B, Ozanam F, Chazalviel J-N, Carstensen J, Föll H, Wehrspohn RB (2005) Electrochem Solid-State Lett 8:B25
26. Mor GK, Shankar K, Paulose M, Varghese OK, Grimes CA (2006) Nano Lett 6:215
27. Choi H, Sofranko AC, Dionysiou DD (2006) Adv Mater 18:1067
28. Song Y, Zhu XF, Wang X, Che J, Du Y (2001) J Appl Electrochem 31:1273